Discordant synchronization patterns on directed networks of identical phase oscillators with attractive and repulsive couplings

Thomas Peron *

Instituto de Ciências Matemáticas e de Computação, Universidade de São Paulo, São Carlos 13566-590, São Paulo, Brazil

(Received 27 January 2021; accepted 23 March 2021; published 15 April 2021)

We study the collective dynamics of identical phase oscillators on globally coupled networks whose interactions are asymmetric and mediated by positive and negative couplings. We split the set of oscillators into two interconnected subpopulations. In this setup, oscillators belonging to the same group interact via symmetric couplings while the interaction between subpopulations occurs in an asymmetric fashion. By employing the dimensional reduction scheme of the Ott-Antonsen (OA) theory, we verify the existence of traveling wave and π-states, in addition to the classical fully synchronized and incoherent states. Bistability between all collective states is reported. Analytical results are generally in excellent agreement with simulations; for some parameters and initial conditions, however, we numerically detect chimera-like states which are not captured by the OA theory.

DOI: 10.1103/PhysRevE.103.042210

I. INTRODUCTION

The Kuramoto model of coupled phase oscillators has become over the years a paradigmatic tool for the study of emergent synchronization phenomena in nonlinear sciences. In its first formulation, globally coupled oscillators interact via the sine of the differences of their phases; this interaction is weighted by a positive coupling strength, and by increasing its magnitude, the phases are gradually pulled towards a common value, creating then a synchronization phase transition [1–3]. Initially conceived as a solvable extension of the model proposed by Winfree [4], the Kuramoto model attracted great attention due to its analytical tractability and its later discovered potential to describe synchronization phenomena in a diverse set of systems, such as in optomechanical cells [5], Josephson junctions [6], chemical oscillators [7], power networks [8], and even the synchrony among violin players [9]. For a long list of examples of the use of Kuramoto models in real applications see the reviews in Refs. [1–3].

Many variations of the original model by Kuramoto have been inspired by particular features found in different physical systems [1]. One example is the seminal work carried out by Daido [10], who, inspired by spin-glass models, treated the couplings between oscillators in a Kuramoto model as random variables which could be either positive or negative. Daido's results provided evidence for an analogous glass phase transition in oscillatory systems; however, the precise conditions for the existence of those "oscillator glasses" have remained unclear, and still some debate surrounds the problem [11–15]. After the early works by Daido and others [10–14,16], the discussion on oscillator glasses was brought back to attention by Hong and Strogatz, who in a series of papers [17–19] further exploited the role of negative and positive couplings. In the first coupling setting considered by them [17,18], oscillators were divided into two globally coupled subpopulations characterized by distinct coupling strengths. In a scenario resembling sociodynamical models, oscillators within the first subpopulation were modeled to have the tendency to align with the mean-field (conformist oscillators), whereas the second subpopulation was defined by oscillators that are repelled by the other units (contrarian oscillators). In the second model [19], a fraction of the oscillators was considered to provide positive coupling inputs to other nodes, while the remainder contributed with negative couplings; that is, in mathematical terms, the coupling variable was placed inside the summation term of the interaction function. Despite being very similar, the two coupling formulations have been shown to yield significantly different collective dynamics; in fact, only the model in Refs. [17,18] was found to lead to different transitions other than between incoherence and classical partially synchronized states.

Although Hong and Strogatz did not bring new evidence to support or discard the existence of oscillator glasses, their papers motivated several other studies on discordant synchronization patterns—i.e., states characterized by the separation of the population of oscillators into partially synchronized clusters—induced by the coexistence of attractive and repulsive couplings (see, e.g., Refs. [15,20–32]). Of particular interest here is the work by Sonnenschein *et al.* [24], where the authors unified the coupling settings of Refs. [17–19] into a single model that also included the influence of stochastic fluctuations on the frequencies. More specifically, in Ref. [24], Kuramoto oscillators were set to interact concomitantly via a coupling K_i, which was placed outside the summation term of the interaction function, regulating the neighboring influence perceived by oscillator i, and a coupling G_i placed inside the sum, endowing the oscillators with the ability to contribute differently to the mean field. By employing the dimension reduction framework offered by the Gaussian approximation

*thomaskaue@gmail.com

[33], the authors showed that all states previously reported in Refs. [17–19] (namely, traveling waves and π-states, and conventional incoherent and synchronous states) persisted in the model with both types of couplings, but under new routes outlining the transitions between different states.

The relevance of mixing positive and negative couplings in phase-oscillator models actually goes beyond the theoretical interest in oscillator glasses: It turns out that certain types of physical, biological, and chemical systems can indeed be described as oscillators coupled through attractive and repulsive interactions. Noteworthy real-world examples showing similar characteristics and phenomena as those described above include laser arrays [34,35] and electrochemical oscillators [36,37]. Furthermore, the balance between phase attraction and repulsion has been recently shown to be a key factor in the regulation of circadian rhythms by pacemakers cells in the suprachiasmatic nucleus (SCN) [38].

Motivated by the aforementioned contributions, here we investigate the model in Ref. [24] of identical oscillators in the absence of stochastic fluctuations acting on the frequencies. We divide the oscillators into two subpopulations asymmetrically coupled, and employ the theory by Ott and Antonsen (OA) [39,40] to obtain a reduced set of equations that describes the evolution of the system. By studying the linear stability of the reduced system, we analytically derive several conditions that delineate the transitions between synchronized, incoherent, traveling waves and π-states. Interestingly, we find the dynamics of the present model to be overall more intricate than its stochastic version [24], with wider regions in the parameter space exhibiting coexistence between different synchronization patterns. As we shall see, simulations with large populations of oscillators in general confirm with excellent agreement the predictions by the theory; for a small set of parameters, however, we report strong deviations from the dynamics yielded by the reduced system.

II. MODEL

Following Sonnenschein *et al.* [24], we study here the system made up of N identical Kuramoto oscillators whose equations are given by

$$\dot{\theta}_i = \omega_0 + \frac{K_i}{N}\sum_{j=1}^{N} G_j \sin(\theta_j - \theta_i), \tag{1}$$

where $i = 1, \ldots, N$, and ω_0 is the natural frequency. Notice that, in contrast to Ref. [24], we do not consider identical oscillators under the influence of stochastic fluctuations in the phase dynamics; instead, the only source of disorder is the one inflicted by the coupling strengths. We henceforth refer to parameters K_i and G_j as the in- and out-coupling strengths, respectively. As defined in Eq. (1), these couplings set the interactions between the oscillators to be asymmetric (or directed): oscillator i contributes to the dynamics of neighboring nodes with weight G_i, while the input arising from other oscillators is weighted by K_i. The first model by Hong and Strogatz [17] is recovered when $G_i = 1 \forall i$ in Eq. (1) (no out-coupling strengths), while the second model investigated by the same authors [19] is obtained by symmetrizing the in-coupling strengths, i.e., $K_i = 1 \forall i$. Bifurcation conditions have been calculated recently for a stochastic system with a coupling scheme similar to Eq. (1) [41]. Other similar forms of the coupling setting of Eq. (1) have also been addressed recently in Refs. [15,42], considering a phase frustration term in the interaction function (Kuramoto-Sakaguchi model [43]) and in populations of asymmetrically coupled Rössler oscillators [44].

III. DIMENSIONAL REDUCTION

In the continuum limit $N \to \infty$, we rewrite the original Eq. (1) by omitting the subindexes as

$$\dot{\theta} = \omega_0 + KR\sin(\Theta - \theta), \tag{2}$$

where R and Θ are the "weighted" order parameter and the mean-field phase, respectively, defined by

$$Re^{i\Theta} = \iint G r_{K,G} e^{i\psi_{K,G}} P(K,G)\, dK\, dG. \tag{3}$$

$P(K,G)$ is the joint distribution of in- and out-coupling strengths; variables $r_{K,G}e^{i\phi_{K,G}}$ are the local order parameters that quantify the synchrony within subpopulations:

$$z_{K,G} = r_{K,G}e^{i\psi_{K,G}} = \int \rho(\theta, t|K,G) e^{i\theta}\, d\theta, \tag{4}$$

where $\rho(\theta, t|K,G)$ is the probability density function of observing an oscillator with phase θ at time t for a given coupling pair (K,G). Henceforth we adopt the notation $\rho_{K,G}(\theta,t) \equiv \rho(\theta,t|K,G)$. The normalization condition $\int_{-\pi}^{\pi} \rho_{K,G}(\theta,t)\, d\theta = 1$ leads to the following continuity equation:

$$\frac{\partial \rho_{K,G}}{\partial t} + \frac{\partial}{\partial \theta}\{\rho_{K,G}[\omega_0 + KR\sin(\Theta - \theta)]\} = 0. \tag{5}$$

Next we expand the phase density $\rho_{K,G}(\theta,t)$ in a Fourier series and apply the ansatz by Ott and Antonsen [39,40] to its coefficients to get

$$\rho_{K,G}(\theta,t) = \frac{1}{2\pi}\left\{1 + \sum_{n=1}^{N}[\alpha_{K,G}(\omega_0,t)]^n e^{in\theta} + \text{c.c.}\right\}, \tag{6}$$

where $\alpha_{K,G}(t) \equiv \alpha(K,G,t)$, and c.c. stands for the complex conjugate. Substituting Eq. (6) into Eq. (5) yields

$$\dot{\alpha}_{K,G} + i\omega_0\alpha_{K,G} + \frac{K}{2}\left(\alpha_{K,G}^2 R - R^*\right) = 0. \tag{7}$$

Inserting Eq. (5) into Eq. (4), we have that the local order parameters become $z_{K,G} = \alpha^*_{K,G}$. Hence, for a general distribution of coupling strengths $P(K,G)$, we get

$$\begin{aligned}
\dot{r}_{K,G} &= \frac{K}{2}\left(1 - r_{K,G}^2\right)\langle\langle G' r_{K',G'}\cos(\psi_{K,G} - \psi_{K',G'})\rangle\rangle, \\
\dot{\psi}_{K,G} &= \omega_0 - \frac{K}{2}\left(r_{K,G} + r_{K,G}^{-1}\right)\langle\langle G' r_{K',G'}\sin(\psi_{K',G'} - \psi_{K,G})\rangle\rangle,
\end{aligned} \tag{8}$$

where $\langle\langle \cdots \rangle\rangle = \iint P(K',G')\cdots dK' dG'$.

The boundaries of the asynchronous state ($R = 0$) can be obtained straightforwardly for arbitrary distributions $P(K,G)$. By considering small perturbations $\delta r_{K,G}$ around the incoherent state $r_{K,G} = 0$, and setting $\psi_{K,G} = 0$, without loss of

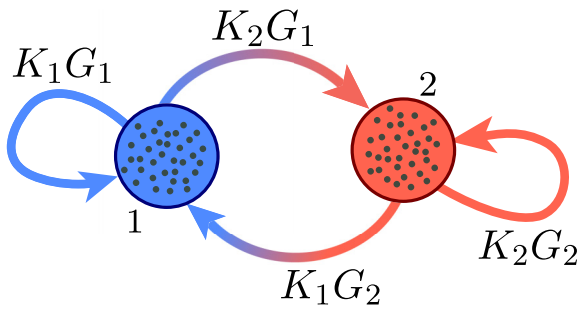

FIG. 1. Schematic illustration of a finite system composed of two intertwined subpopulations. Oscillators belonging to subpopulation 1 (2) interact among themselves via couplings K_1G_1 (K_2G_2), while oscillators from different subpopulations interact asymmetrically with effective couplings K_1G_2 and K_2G_1, as depicted in the figure.

generality, we get from Eq. (8)

$$\dot{\delta r}_{K,G} = \frac{K}{2}\langle\langle G'\delta r_{K',G'}\rangle\rangle. \tag{9}$$

By multiplying the previous equation by G and averaging over the distribution $P(K,G)$, we rewrite Eq. (9) in terms of a perturbation to the global order parameter $\delta R = \langle\langle G'\delta r_{K',G'}\rangle\rangle$, $\dot{\delta R} = [\langle\langle KG\rangle\rangle/2]\delta R$, which leads to the critical condition

$$\langle\langle KG\rangle\rangle = 0. \tag{10}$$

Therefore, for $\langle\langle KG\rangle\rangle < 0$, the oscillators remain incoherent, while for $\langle\langle KG\rangle\rangle > 0$ the incoherent state loses stability, and a partially synchronized state sets in. Notice that Eq. (10) is similar to the condition obtained in Ref. [24] for identical oscillators subjected to Gaussian noise.

Let us consider now the case in which the oscillators are coarse-grained into n intertwined subpopulations with joint distribution of couplings given by $P(K,G) = \frac{1}{n}\sum_{q=1}^{n}\delta[(K,G)-(K_q,G_q)]$. Substituting the previous expression for $P(K,G)$ into Eqs. (8) yields

$$\begin{aligned}\dot{r}_q &= -\frac{K_q}{2n}\left(1-r_q^2\right)\sum_{p=1}^{n} G_p r_p\cos(\psi_p-\psi_q),\\ \dot{\psi}_q &= \omega_0 - \frac{K_q}{2n}\left(r_q+r_q^{-1}\right)\sum_{p=1}^{n} G_p r_p\sin(\psi_p-\psi_q),\end{aligned} \tag{11}$$

where $q = 1,\ldots,n$. In what follows we investigate a special case of the above system, namely, the setup of two intertwined subpopulations [24]. In this case, we have $n = 2$, and Eqs. (11) are reduced to

$$\begin{aligned}\dot{r}_1 &= \frac{K_1}{4}\left(1-r_1^2\right)[r_1G_1 + r_2G_2\cos\delta],\\ \dot{r}_2 &= \frac{K_2}{4}\left(1-r_2^2\right)[r_2G_2 + r_1G_1\cos\delta],\\ \dot{\delta} &= -\frac{\sin\delta}{4}\left[\left(r_1+r_1^{-1}\right)r_2K_1G_2 + \left(r_2+r_2^{-1}\right)r_1K_2G_1\right],\end{aligned} \tag{12}$$

where we have defined the phase lag $\delta = \psi_1 - \psi_2$. An illustration of a finite network with two intertwined subpopulations can be seen in Fig. 1. We measure the global synchronization with the classical Kuramoto order parameter as

$$r(t)e^{i\Phi(t)} = \tfrac{1}{2}[r_1(t)e^{i\psi_1(t)} + r_2(t)e^{i\psi_2(t)}]. \tag{13}$$

Note that $r(t)e^{i\Phi(t)}$ in the above equation is different from the "weighted" order parameter $Re^{i\Theta} = \frac{1}{2}[r_1(t)G_1e^{i\psi_1(t)} + r_2(t)G_2e^{i\psi_2(t)}]$ [Eq. (3)], which can be larger than one.

Equations (12) are very similar to the set of equations for identical oscillators under the influence stochastic fluctuations obtained via Gaussian approximation [24,33]. Actually, the only difference between the reduced system obtained in Ref. [24] and Eqs. (12) is that the former exhibits terms $r_{1,2}^4$ instead of $r_{1,2}^2$ in the equations for $\dot{r}_{1,2}$ and terms proportional to $(r_{1,2}^{-1}+r_{1,2}^3)$ in place of $(r_{1,2}^{-1}+r_{1,2})$ in the equation for $\dot{\delta}$. Notice also that Eqs. (12) could be obtained via the Watanabe-Strogatz theory [45,46] under uniform distribution of constants of motion (Ott-Antonsen manifold) [18,40,47].

From Eqs. (12), we expect to observe the following stationary states for the two subpopulation system (see the illustration in Fig. 2): (1) the classical incoherent state in which $r = r_{1,2} = 0$; (2) the perfectly synchronized state in which $r_{1,2} = 1$ and $\delta = 0$ (we denominate this state as a "zero-lag sync" state); (3) partially synchronized states characterized by $r_{1,2} < 1$ and $\delta = 0$, which we refer to as "blurred zero-lag sync" states; (4) the so-called "π-state" for which the subpopulations are perfectly synchronized ($r_{1,2} = 1$), while remaining diametrically opposed in the phase space ($\delta = \pi$), yielding, hence, a vanishing global synchronization ($r = 0$); (5) "blurred" π-states, in which at least one of the subpopulations is partially synchronized ($r_{1,2} < 1$) and the peaks of their phase distributions are separated by $\delta = \pi$; and, finally, (6) the traveling-wave (TW) state [17,24,48] in which the subpopulations can be either partially or fully synchronized, $0 < r_{1,2} \leqslant 1$, while keeping a constant phase-lag separation within $0 < \delta < \pi$. The interesting feature of this state is that, in contrast to standard formulations of the Kuramoto model, the oscillators no longer rotate with a common frequency given by the frequency ω_0 of the corotating frame—or $\bar{\omega} = \int \omega g(\omega)\, d\omega$ in the case of nonidentical oscillators, where $g(\omega)$ is a frequency distribution [17,48]; instead, they settle on a new stationary rhythm whose magnitude will also depend on the coupling parameters. Deviations from the mean frequency $\bar{\omega}$ can be calculated either by the average (or mean-ensemble) frequency

$$\Omega = \frac{1}{N}\sum_{j=1}^{N}\langle\dot{\theta}_j\rangle_t, \tag{14}$$

where $\langle\cdots\rangle_t$ denotes a long-time average or by the locking frequency $\dot{\Theta}$, defined in Eq. (3) [see also Eq. (18)]. TW states typically appear in phase-oscillator systems when certain symmetry patterns are broken in the model, such as by the presence of a phase frustration in the sine coupling term [43], asymmetric coupling strength distributions [17,18], or natural frequencies asymmetrically distributed [48].

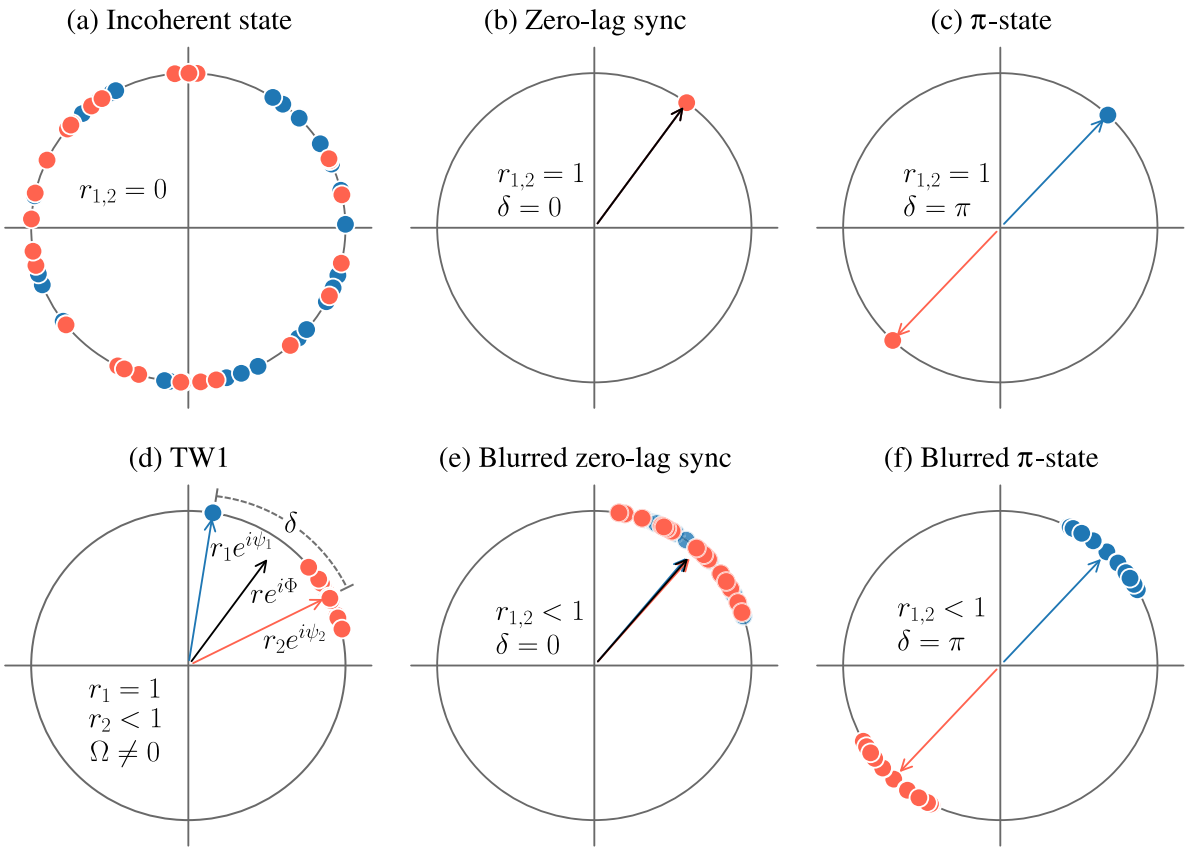

FIG. 2. Long-time profile on the complex unit circle of the states observed for a finite system [Eq. (1)] with two intertwined subpopulations coupled as depicted in Fig. 1: (a) Incoherent state, (b) zero-lag sync, (c) π-state, (d) TW1, (e) blurred zero-lag sync, and (f) blurred π-state. Only in the TW1 state (d), the collective frequencies $\dot{\Theta}$ [Eq. (18)], $\dot{\Phi}$ [Eq. (13)] and Ω [Eq. (14)] are different from zero, and the oscillators travel across all possible phase values in the corotating frame defined by the natural frequency. The configuration of the TW2 state is obtained by interchanging the subindexes and colors in panel (d).

IV. BIFURCATION ANALYSIS OF THE REDUCED SYSTEM WITH TWO SUBPOPULATIONS

For convenience, we adopt the following parametrization for the couplings:

$$K_{1,2} = K_0 \pm \frac{\Delta K}{2} \text{ and } G_{1,2} = G_0 \pm \frac{\Delta G}{2}, \tag{15}$$

where K_0 and G_0 are the average in- and out-coupling strengths, respectively; parameters ΔK and ΔG are defined as the corresponding coupling mismatches. In our calculations we always consider positive mismatches (ΔK, $\Delta G > 0$). Therefore, if $|K_0| < |\Delta K|/2$ or $|G_0| < |\Delta G|/2$, half of the couplings are positive (attractive) and half are negative (repulsive). If one of these conditions is satisfied, we say that the oscillators interact via *mixed couplings*.

By setting $\dot{\delta} = 0$, we uncover two possible fixed-point solutions for phase lag δ:

$$\delta = m\pi, m \in \mathbb{Z}, \tag{16}$$

$$0 = \left(r_1 + r_1^{-1}\right) r_2 K_1 G_2 + \left(r_2 + r_2^{-1}\right) r_1 K_2 G_1. \tag{17}$$

Equation (16) corresponds to the solution of partially synchronized states with no separation between populations (even m) and π-states (odd m), while Eq. (17) gives the condition for the existence of TW states. We can verify that TWs appear only for $0 < \delta < \pi$ by rewriting the equations for $\dot{\psi}_{1,2}$ together with Eq. (17) as

$$\lim_{t\to\infty} \dot{\psi}_{1,2} = \lim_{t\to\infty} \dot{\Theta} = \omega_0 - \sin\delta \frac{r_2 + r_2^{-1}}{4} K_2 G_1 r_1. \tag{18}$$

Therefore, spontaneous drifts in the collective frequencies occur only for intermediate values of the phase lag δ; otherwise, for $\delta = m\pi$, oscillators rotate with collective frequencies $\dot{\psi}_{1,2} = \omega_0$, which here is set to $\omega_0 = 0$.

From the parametrization in Eq. (15), we realize the critical conditions $K_{1,2} = 0$, or

$$K_0 = \pm \frac{\Delta K}{2}. \tag{19}$$

When one of the above conditions holds, it follows that one subpopulation is deprived of receiving inputs from other nodes (including from the same subpopulation), and its oscillators have instead only out-couplings towards nodes external to their subpopulation. Similarly, if one of the out-couplings vanishes, $G_{1,2} = 0$, the corresponding subpopulation ceases to influence the dynamics of the rest of the network and starts acting only as a link receiver. As we shall see, these conditions play an important role in the phase diagram of Eqs. (12). In the

sequel, we calculate the coupling ranges in which the states discussed in the previous section appear.

A. Incoherent state

The first critical condition of Eqs. (12) is given by the stability analysis of the incoherent state performed in the last section. For the case of two subpopulations with $P(K,G)=\frac{1}{2}\delta[(K,G)-(K_1,G_1)]+\frac{1}{2}\delta[(K,G)-(K_2,G_2)]$, Eq. (10) reads $K_1G_1+K_2G_2=0$, and by solving it in terms of the average in-coupling strength we have

$$K_0=-\frac{\Delta K\Delta G}{4G_0}. \tag{20}$$

The above equation, therefore, delineates the boundary of the incoherent state.

B. π-states

For the π-state, the fixed point solutions read $r_{1,2}=1$ and $\delta=\pi$. Linear stability reveals that the π-state is stable for average in-couplings given by

$$\begin{aligned}-\frac{\Delta K}{2}<K_0<\min\left\{\frac{\Delta K}{2},\frac{\Delta K\Delta G}{4G_0}\right\},\ \text{for } G_0>0;\\ \max\left\{-\frac{\Delta K}{2},\frac{\Delta K\Delta G}{4G_0}\right\}<K_0<\frac{\Delta K}{2},\ \text{for } G_0<0.\end{aligned} \tag{21}$$

The other state characterized by subpopulations diametrically opposed is the blurred π-state, and its fixed points are defined by $r_1G_1=r_2G_2$ and $\delta=\pi$. Linearizing the dynamics about this state, we find that the corresponding Jacobian matrix has a single nonzero eigenvalue, $\lambda=K_1G_1(1-r_1^2)/4+K_2G_2(1-r_2^2)/4$. Hence, and because couplings G_1 and G_2 must have the same sign so that $r_1G_1=r_2G_2$ is a physical solution, we have that blurred π-states appear when

$$K_0<\frac{\Delta K\Delta G}{4G_0},\ \text{for } |G_0|>\frac{\Delta G}{2}. \tag{22}$$

Thus, both π-states with fully synchronous subpopulations ($r_{1,2}=1$) and with partial synchronization ($r_{1,2}<1$) are yielded by systems described by Eqs. (12). Observe also that $r_1G_1=r_2G_2$ defines a one-parameter family of fixed points. Furthermore, from Eq. (22) we notice that incoherent and blurred π-states may coexist in a large region of the parameter space defined by coupling strengths G_0 and K_0.

C. Zero-lag sync and partially synchronized states

For the zero-lag sync state, we linearize Eqs. (12) around $r_{1,2}=1$ and $\delta=0$, and seek a zero eigenvalue of the related Jacobian matrix. By following this calculation, we find that the zero-lag sync state emerges for average in-coupling strengths given by

$$\begin{aligned}K_0>\max\left\{\frac{\Delta K}{2},\frac{\Delta K\Delta G}{4G_0}\right\},\ \text{for } G_0>0;\\ K_0<\min\left\{-\frac{\Delta K}{2},\frac{\Delta K\Delta G}{4G_0}\right\},\ \text{for } G_0<0.\end{aligned} \tag{23}$$

Next, by linearizing Eqs. (12) around an arbitrary partially synchronized solution ($r_1G_1=-r_2G_2$ and $\delta=0$), we find that such states, which we have denominated blurred zero-lag sync states, must occur for parameters in the range

$$K_0<\frac{\Delta K\Delta G}{4G_0},\ \text{for } |G_0|<\frac{\Delta G}{2}. \tag{24}$$

Any state that satisfies $r_1G_1=-r_2G_2$ and $\delta=0$ is a fixed point of Eqs. (12). From this we foresee that several partially synchronized states should coexist in the region delimited by Eq. (24). As in the case of blurred π-states, blurred zero-lag sync solutions yield a single nonzero Jacobian eigenvalue, $\lambda=K_1G_1(1-r_1^2)/4+K_2G_2(1-r_2^2)/4$; hence, the latter states do not coexist with zero-lag sync or with π-states, because in regions where $r_{1,2}=1$ we have $\lambda=0$, and the blurred zero-lag sync states lose stability. Notice further that in order to $r_1G_1=-r_2G_2$ be a physical solution, out-couplings G_1 and G_2 must have opposite signs; thus, partially synchronized states with $\delta=0$ are expected to appear only in the presence of mixed-out coupling strengths, i.e., for $|G_0|<\Delta G/2$, as indicated in Eq. (24).

D. Traveling waves

We now turn our attention to the stationary TW states. Numerical results show us that two possible TW states are manifested by the system (12). In the first state, which we refer to as "TW1," the first subpopulation remains fully synchronized ($r_1=1$), whereas the second one exhibits partial synchronization ($r_2<1$). We label as "TW2" the opposite situation, i.e., when $r_2=1$ and $r_1<1$. In both states we have $0<\delta<\pi$ and $\Omega>0$. By setting $r_1=1$ in Eqs. (12), we find the following fixed point solutions for r_2 and δ:

$$r_2=\sqrt{-\frac{K_2G_1}{K_2G_1+2K_1G_2}}\ \text{and}\ \cos\delta=-\frac{G_2}{G_1}r_2. \tag{25}$$

Since $0<r_2<1$, we have that the solution of the TW1 exists for

$$-K_1G_2<K_2G_1<0. \tag{26}$$

By writing Eq. (26) in terms of the parametrization in Eq. (15), and considering $\Delta K,\Delta G>0$, we find that the regions with TW1 are outlined by the following conditions:

$$\frac{\Delta K\Delta G}{4G_0}<K_0<\frac{\Delta K}{2},\ \text{for } G_0>\frac{\Delta G}{2}. \tag{27}$$

The linearization of Eqs. (12) about the fixed points of Eq. (25) also reveals a second region in which the TW1 state is stable:

$$\begin{aligned}\frac{\Delta K}{2}<K_0<\frac{\Delta K}{8}\left[\frac{\Delta G}{G_0}\right]^2,\ \text{for } -\frac{\Delta G}{2}<G_0<0;\\ \frac{\Delta K}{2}<K_0<\frac{\Delta K\Delta G}{4G_0},\ \text{for } 0<G_0<\frac{\Delta G}{2}.\end{aligned} \tag{28}$$

The solutions for r_1 and δ, and the critical conditions for the TW2 state are obtained by interchanging the indexes "1" and "2" in Eqs. (25) and (26). By following the same procedure for the corresponding TW2 solutions, one uncovers that this

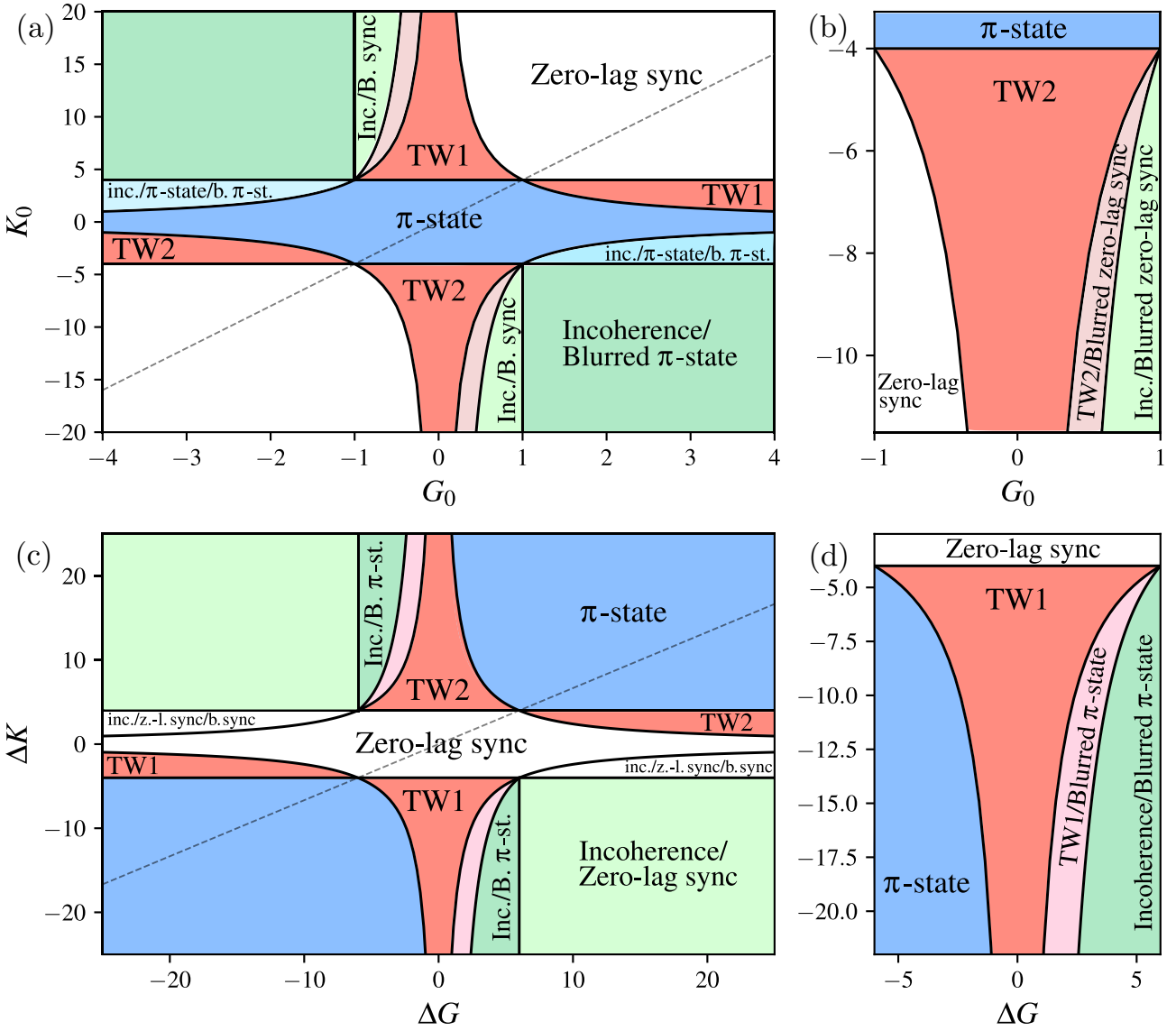

FIG. 3. Bifurcation diagram of the reduced system [Eqs. (12)] for (a, b) $\Delta K = 8$ and $\Delta G = 2$; and (c, d) $K_0 = 3$ and $G_0 = 2$. Zero-lag sync corresponds to the perfectly synchronized state ($r_{1,2} = 1$ and $\delta = 0$). "π-state" refers to the state in which $r_{1,2} = 1$ and phase-lag separation $\delta = \pi$. Similarly, blurred zero-lag and blurred π-states denote the states with $r_{1,2} < 1$ along with $\delta = 0$ and $\delta = \pi$, respectively. Traveling wave states are characterized by $r_1 = 1$, $r_2 < 1$ (TW1), and $r_2 = 1$, $r_1 < 1$ (TW2). Both TW1 and TW2 exhibit $\Omega \neq 0$ [Eq. (14)]. Solid lines are obtained from Eqs. (20)–(24) and Eqs. (27)–(29). Dashed line in panels (a) and (c) depict the condition $K_0\Delta G - \Delta K G_0 = 0$ for which the couplings are symmetric, i.e., when the network connections are undirected. Panels (b) and (d) show zoomed-in regions of panels (a) and (c), respectively.

state appears for average in-coupling strengths given by

$$
\begin{aligned}
-\frac{\Delta K}{2} < K_0 < \frac{\Delta K \Delta G}{4G_0}, \text{ for } G_0 < -\frac{\Delta G}{2};\\
\frac{\Delta K \Delta G}{4G_0} < K_0 < -\frac{\Delta K}{2}, \text{ for } -\frac{\Delta G}{2} < G_0 < 0;\\
-\frac{\Delta K}{8}\left[\frac{\Delta G}{G_0}\right]^2 < K_0 < -\frac{\Delta K}{2}, \text{ for } 0 < G_0 < \frac{\Delta G}{2}.
\end{aligned}
\tag{29}
$$

Alternatively, the conditions of the TW2 state [Eqs. (29)] could be obtained by letting $(\Delta K, \Delta G) \to (-\Delta K, -\Delta G)$ in the TW1 conditions [Eqs. (27) and (28)].

Figure 3(a) depicts the bifurcation diagram outlined by the critical conditions in Eqs. (20)–(24) and Eqs. (27)–(29). As can be seen, for high values of both K_0 and G_0, the dynamics converges either to perfect synchronization or to incoherence/blurred π-state; for intermediate values, however, multiple regions of bistability appear. Interestingly, although simpler, the model in Eq. (1) exhibits a more complex dynamics than its stochastic version [24]. By comparing the diagrams of Fig. 3 with their counterparts in Ref. [24], we see that the regions with coexistence between different states become proportionally larger when noise is absent. A similar effect was observed by Hong and Strogatz when comparing the findings in Refs. [17,18].

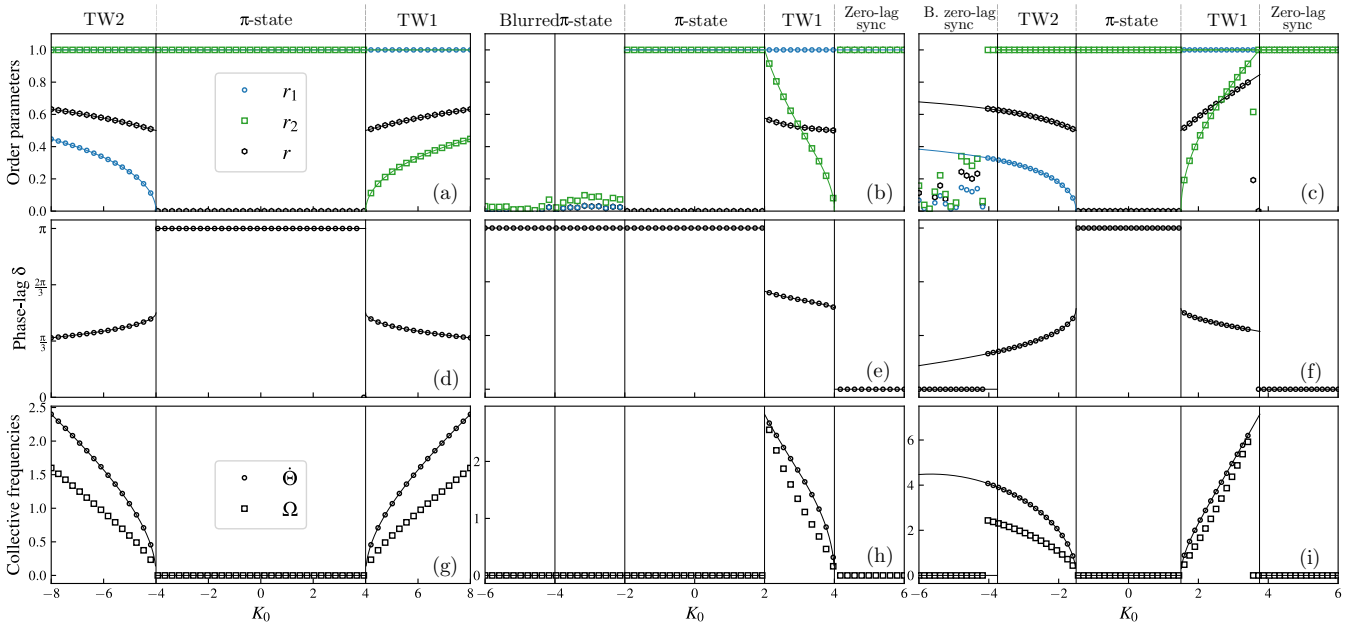

FIG. 4. Order parameters $r_{1,2}$, r, phase lag δ, and collective frequencies $\dot{\Theta}$ [Eq. (18)] and Ω [Eq. (14)] for (a, d, g) $G_0 = 0$, $\Delta K = 8$, and $\Delta G = 2$; (b, e, h) $G_0 = 2$, $\Delta K = 8$, and $\Delta G = 2$; and (c, f, i) $G_0 = 2$, $\Delta K = 3$ and $\Delta G = 10$. Dots are obtained by numerically integrating the original system [Eq. (1)] using Heun's method with $N = 10^4$ oscillators. For each coupling value K_0, the quantities are averaged over $t \in [500, 1500]$ with a time step $dt = 0.005$. In all panels, initial conditions $\theta_i(t = 0)$ $\forall i$ are randomly distributed according to a uniform distribution between $[-\pi, \pi]$. Solid lines correspond to the analytic solutions obtained in Sec. IV.

By rewriting the critical couplings in Eqs. (20)–(24) and Eqs. (27)–(29) in terms of coupling mismatches, we derive the stability diagram spanned by the parameters ΔG and ΔK. Similarly to what was verified in Ref. [24], the arrangement of the transitions in Fig. 3 evidences some rules for the occurrence of the collective states manifested by the system (1). First, in order to observe π-states, mixed in-couplings are required [see the blue areas in Fig. 3(c) occurring for $\Delta K > 2K_0$]. States TW1 and TW2 emerge when either mixed in- or out-coupling exist, but never when both types of couplings are mixed; in the latter case, only incoherence and π-states are possible. Bistability of TWs and incoherence with π-states appear when mixed in-coupling strengths exist, whereas we observe bistable regions TW or zero-lag sync and TW or incoherence when only out-couplings are mixed. Finally, we emphasize the importance of the directness in the network connections for the emergence of traveling waves. For $K_0\Delta G - \Delta K G_0 = 0$, the coupling strengths connecting the subpopulations become equal, and the interaction is no longer asymmetric. By projecting this expression onto the stability diagram (see the dashed lines in Fig. 3), we see that the symmetry condition does not intersect TW regions; therefore, asymmetric interactions are necessary for the emergence of such states. Nevertheless, as seen in Fig. 3, π-states are crossed by the line imposed by the symmetry relation, meaning that asymmetric couplings are not required for the existence of π-states.

The diagrams in Fig. 3 also allow us to reexamine the results in Refs. [17–19] as particular cases of the present model. As mentioned previously, in Refs. [17,18], the authors studied Kuramoto oscillators subjected to attractive and repulsive in-couplings strengths ($\Delta G = 0$ in our notation). In that setting, the couplings are regarded as a property of the nodes; thus, a fraction of the oscillators tends to align with the mean field (conformists oscillators), while the rest is repelled by it (contrarian oscillators). As shown in Refs. [17,18], the absence of out-coupling strengths does not impede the system from reaching π-states and traveling waves. Indeed, if we set $\Delta G = 0$ in Fig. 3(c) and follow the transitions along the K_0-axis, we see that the system switches from TW1 to TW2 via crossing the central zero-lag sync area. In their follow-up study [19], the couplings were treated as properties of the links, that is, the coupling terms were placed inside the summation over the neighbors' connections instead of outside as in Refs. [17,18]. This coupling setting is equivalent to the model in Eq. (1) in the absence of in-coupling strength mismatches ($\Delta K = 0$). Interestingly, despite the presence of mixed couplings, neither traveling waves nor π-states were detected, but rather only partially synchronized and incoherent states [19]. The fact that mixed out-couplings under no mismatch in the in-couplings yield only a classical mean-field behavior is evident in Fig. 3, where we see that for $\Delta K = 0$ the only possible state is zero-lag sync.

V. SIMULATIONS

Let us now compare the results of the bifurcation analysis in the previous section with numerical simulations of the finite original dynamics [Eq. (1)]. Figure 4 shows the evolution of order parameters, phase-lag separation δ, and collective frequencies, Ω and $\dot{\Theta}$, as a function of K_0 for different choices of G_0. All the simulations are performed by integrating Eq. (1) with Heun's method with a time step $dt = 0.005$ and considering total number of oscillators $N = 10^4$ (see the caption

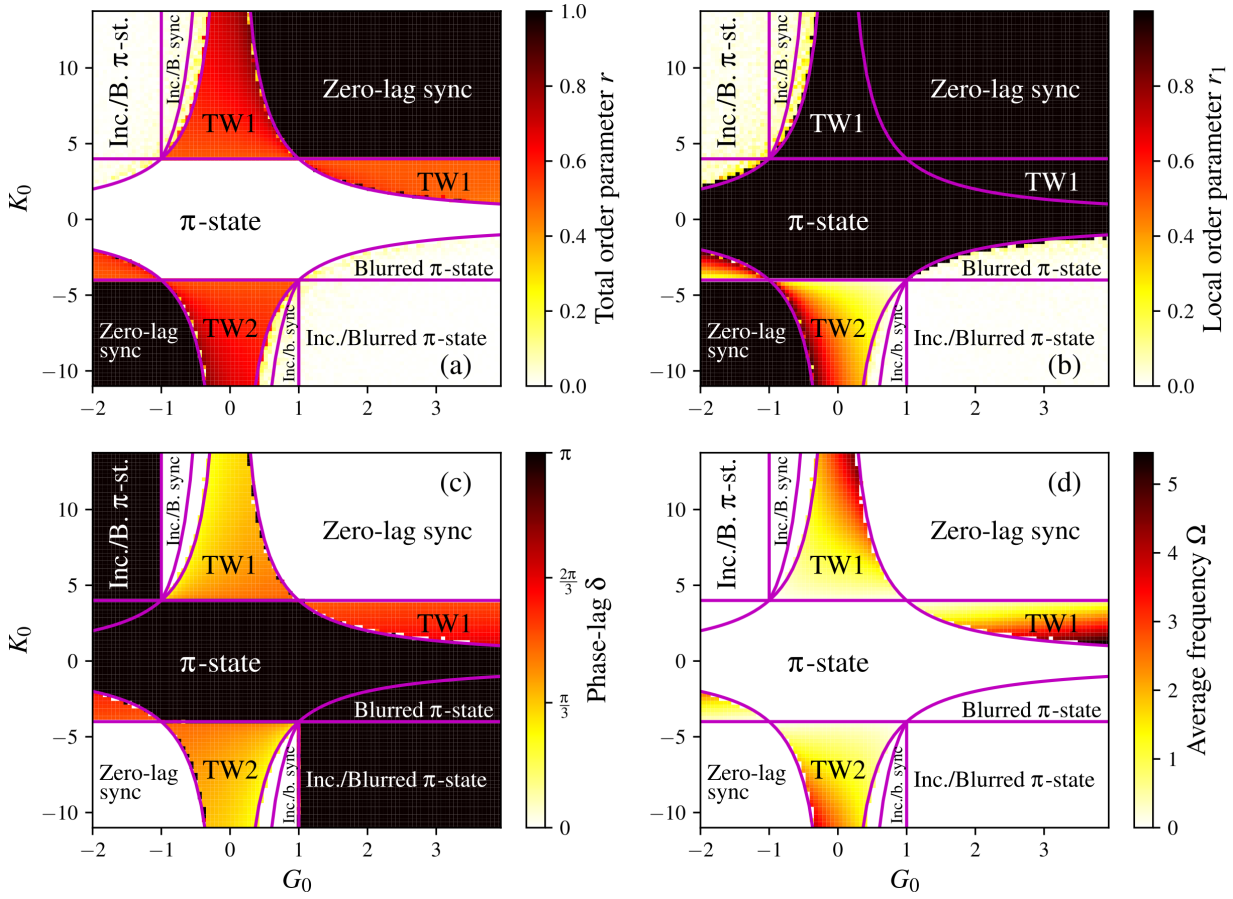

FIG. 5. Comparison between simulations (colormaps) and theory (solid lines). (a) Total order parameter r; (b) local order parameter r_1 of subpopulation 1; (c) phase lag δ measuring the separation between the two subpopulations; and (d) average frequency Ω [Eq. (14)]. For each pair of couplings (G_0, K_0), Eq. (1) is evolved numerically with the Heun's method considering $N = 10^4$ oscillators and with an integration time step $dt = 0.005$. The long-time behavior of each parameter is quantified by averaging the trajectories over $t \in [500, 1000]$. For all (G_0, K_0), the initial phases $\theta_i(t = 0)$ are drawn uniformly at random over the interval $[-\pi, \pi]$. Coupling mismatch parameters: $\Delta K = 8$ and $\Delta G = 2$. $G_0 \times K_0$ grid resolution: 100×100 couplings

of Fig. 4 for more details). This value for the system size was chosen so that temporal fluctuations due to finite-size effects of $O(N^{-1/2})$ become negligible in comparison to the magnitude of r and $r_{1,2}$. For $G_0 = 0$ [Figs. 4 (a), 4(d), and 4(g)] we observe that the system transitions from TW2 to π-state, and then subsequently to TW1, as correctly predicted by the critical conditions depicted in the diagram of Fig. 3. In Fig. 4(b) we see that at $K_0 = -2$ the subpopulations abruptly synchronize as they switch from blurred π-states to π-state. A similar discontinuous transition of the local order parameters $r_{1,2}$ was observed for similar parameter configurations in the stochastic version of the system (1) [24]. Abrupt transitions are also seen in Fig. 4(c), but this time as a consequence of the transition from blurred zero-lag sync to TW2 state. In Fig. 4(c) we also observe irregular points in the "B. zero-lag sync" region. Those points correspond to partially synchronized states and display such an irregular pattern because of the one-parameter family of solutions that exists in that region; specifically, different initial conditions drive the system to different stationary states that satisfy $r_1 G_1 = -r_2 G_2$. The solid branches in "B. zero-lag sync" area correspond to TW2 solutions, which are also stable for $K_0 \lesssim -3.9$ in Fig. 4(c) [see also Fig. 3(b)], but are not obtained numerically with the initial conditions used in Fig. 4. We shall return to this point shortly.

Notice in Figs. 4(g)–4(i) that $|\Omega| \leqslant |\dot{\Theta}|$. The reason for this resides in the fact that Ω is a microscopic average of the instantaneous frequencies $\langle \dot{\theta}_i \rangle$, while $\dot{\Theta}$ [and equivalently $\dot{\Phi}$ in Eq. (13)] quantifies how fast the center of the bulk formed by entrained oscillators rotates. Therefore, oscillators that are not locked with the mean-field contribute to the sum in Eq. (14) with $\langle \dot{\theta}_i \rangle_t \approx 0$, thus reducing the value of Ω in comparison with its upper bound $\dot{\Theta}$. The latter frequency offers in the present case the slight advantage of being calculated directly from the solutions in Eq. (18). Analogously, Ω can be estimated analytically (not shown here) through the ensemble average $\Omega = \int_{-\pi}^{\pi} \iint \dot{\theta}\, \rho(\theta, t|K, G)\, P(K, G)\, dK\, dG\, d\theta$.

To conclude this section, in Fig. 5 we compare the theoretical results with simulations considering coupling parameters over a $G_0 \times K_0$ grid. Our goal with this approach is to inspect for a larger set of parameters whether the analysis performed in the previous section correctly predicts the stability regions shown in Fig. 3. For each coupling pair (G_0, K_0), Eq. (1) is integrated numerically, and the global variables are averaged over $t \in [500, 1500]$ with a time step $dt = 0.005$. As can be seen in Fig. 5, the boundaries of the collective states are

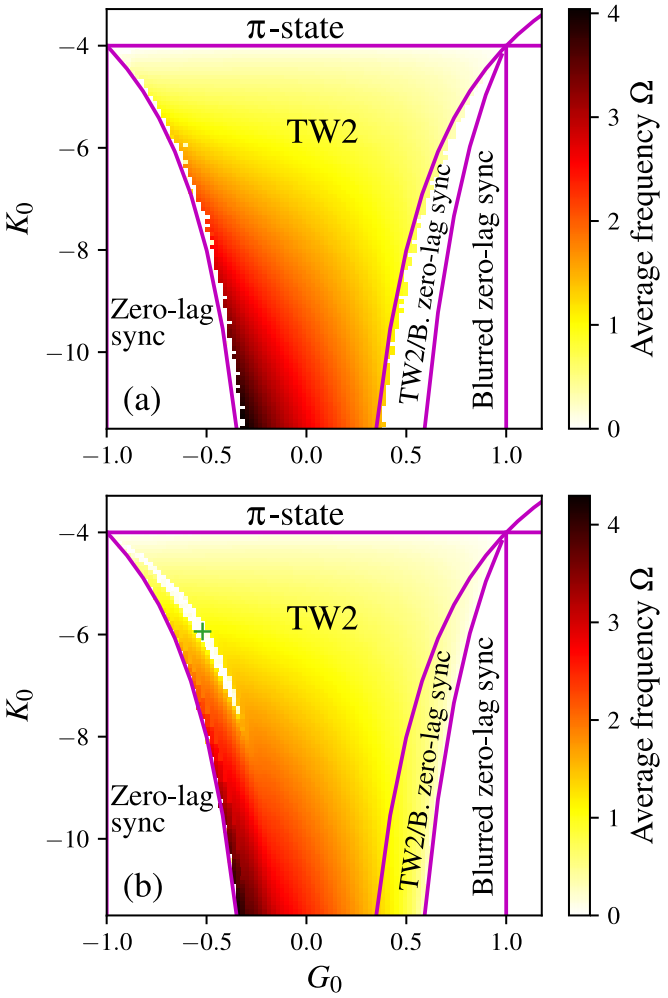

FIG. 6. Comparison between simulations (colormaps) and theory (solid lines) for different sets of initial conditions: (a) $\theta_i(t=0)$ randomly chosen from the uniform distribution $[-\pi,\pi]$ (same as in Fig. 5); (b) for each coupling pair (G_0, K_0) the initial phases of subpopulations 1 and 2 were drawn from Gaussian distributions with standard deviation $\sigma = 2$, and means θ_1 and θ_2, respectively, which were chosen uniformly at random between $[-\pi,\pi]$. The "+" marks a point in the diagram for which the behavior observed in the simulation departs from the dynamics predicted by the theory. Figure 7 shows the temporal evolution of the collective variables at the "+" point depicted in panel (b). Other parameters: $N = 10^4$, $\Delta K = 8$ and $\Delta G = 2$. In both panels the resolution of the grid is 100×100 couplings. Integration was performed with Heun's method using a time step $dt = 0.005$.

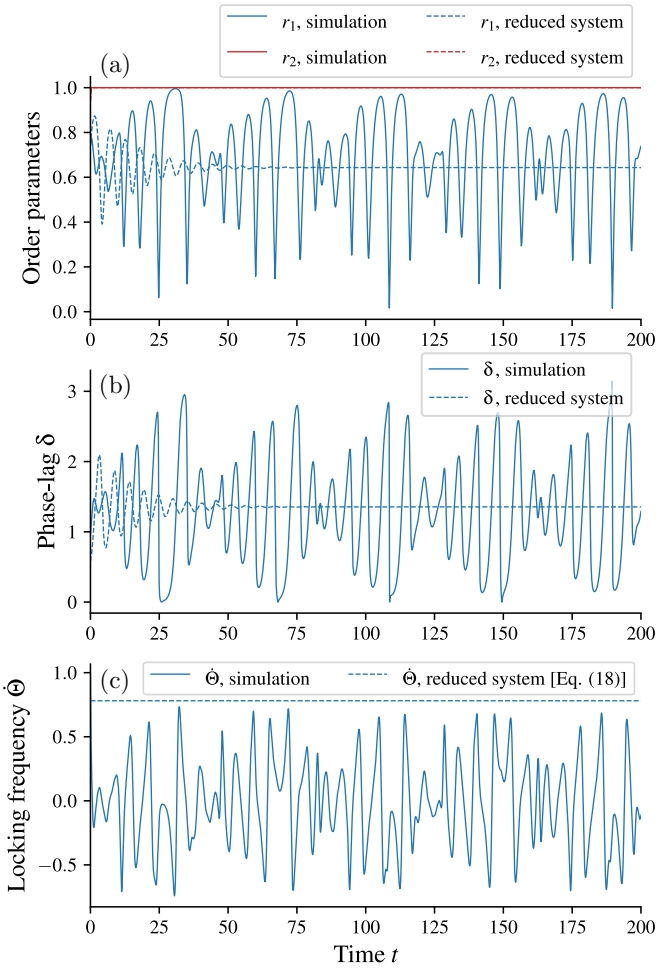

FIG. 7. Temporal evolution of (a) local order parameters $r_{1,2}$, (b) phase lag δ, and (c) locking frequency $\dot{\Theta}$ [Eq. (18)]. Solid lines are obtained from simulations, while dashed lines correspond to the results yielded by the numerical integration of the reduced system [Eq. (12)]. In panel (a) the solid and dashed lines of r_2 overlap each other at $r_2 = 1$. Average in- and out-coupling strengths are taken from the "+" point in Fig. 6(b), that is, $(G_0, K_0) = (-0.5, -5.95)$. Other parameters: $N = 10^4$ oscillators, $\Delta K = 8$, $\Delta G = 2$, and $dt = 0.005$.

predicted very accurately by the theory. Seeking to verify the bistable behavior of the model, in Fig. 6 we show simulations results for a zoomed region of the space in Fig. 5 considering different initial conditions: in Fig. 6(a), phases θ_i are initiated with values distributed uniformly at random between $[-\pi,\pi]$. Initial conditions were chosen differently for Fig. 6(b); specifically, for each point in the grid $G_0 \times K_0$, the phases of populations 1 and 2 were chosen from Gaussian distributions with standard deviation $\sigma = 2$, and means θ_1 and θ_2, which were taken uniformly at random between $[-\pi,\pi]$. By initiating the oscillators in this way, we observe in Fig. 6 that the system converges to TW2 in the region where this state was predicted to coexist with partial synchronization.

VI. ACCURACY OF THE OTT-ANTONSEN REDUCTION

Although we have observed a good agreement between simulations and the theory for the states previously discussed, there are also dynamical patterns which seem not to be captured by the OA reduction. Figure 6 shows an example: there we observe a set of points with $\dot{\Theta} = 0$ in the TW2 area, i.e., a region where one would expect stationary states with $\dot{\Theta} \neq 0$. By inspecting the temporal trajectories of the local order parameters $r_{1,2}$ in Fig. 7 we see that such states do have a different nature from traveling waves. The trajectories in Fig. 7 actually resemble *breathing chimera* states [49] in which one subpopulation remains fully locked, while the other exhibits an oscillating synchrony. In the figure, we compare the time

evolution of the original model [Eq. (1)] with the numerical integration of the reduced system [Eq. (12)] using the same initial conditions. As it is seen, while the finite subpopulation 1 shows oscillating synchrony, the solution provided by the theory converges to a constant value. Although chimera states have been studied extensively with the OA reduction, Figs. 6 and 7 suggest that such solutions in the present model might lie outside the OA manifold. Interestingly, Refs. [17,18,24] did not report solutions akin to the ones shown in Fig. 7. Actually, in light of the recent results by Engelbrecht and Mirollo [50], we may expect even more complicated states to emerge off the OA manifold. As demonstrated in Ref. [50], the dynamics of multipopulation systems such as the one considered here is often more complex off the OA manifold than on it. Thus, the technique of multiple Poisson manifolds discussed in Ref. [50] offers a way to address the shortcomings of the analyses restricted to the Poisson and OA manifolds, and may thereby unravel phenomena that might have remained undetected with other methods.

VII. CONCLUSION

In this paper we have studied a variant of the Kuramoto model in which identical oscillators are coupled via in- and out-coupling strengths, which in turn can have positive and negative values. Similarly to the setting considered in Ref. [24], heterogeneity in the interactions was introduced by dividing the oscillators into two mutually coupled subpopulations (each one characterized by a distinct pair of couplings), so that connections within the same subpopulation remain symmetric, while connections between subpopulations are asymmetric. In the infinite size limit, we applied the theory by Ott and Antonsen [39] to obtain a reduced set of equations. With the reduced description of the original system, we performed a thorough bifurcation analysis whereby a rich dynamical behavior was revealed. We showed that the present system exhibits different types of π-states and traveling waves, along with classical incoherent and partially synchronized states. Though the transitions among these states bear some similarity to those uncovered for the model with Gaussian white noise in Ref. [24], we have found that our model exhibits a more intricate long-term dynamics than that of observed for its noisy version. The reason for this conclusion resides in the different types of π- and zero-lag sync states uncovered here (which may consist of either perfectly or partially synchronized subpopulations), and in the observation of wider regions in the parameter space displaying bistability. These findings for the seemingly simpler system are in line with previous studies [17,18] comparing the dynamics of identical oscillators with that of nonidentical ones. [Although the system in Eq. (1) and the one of Ref. [24] are both models of identical oscillators, the inclusion of Gaussian white noise yields equivalent phenomenology—with respect to the linearized dynamics—to the case of phase oscillators with natural frequencies drawn from Lorentzian distributions; see the discussion in Ref. [51].]

Despite the excellent agreement between simulations and theory, for a small set of parameter combinations we verified dynamical states which turned out not to be reproduced by the reduced system. As discussed in Sec. VI, we verified vanishing values for the temporal average of the mean-field frequency for couplings inscribed in a TW region. By visualizing the time series of such unanticipated states, we found that one local parameter evolved with an oscillatory dynamics akin to breathing chimera states [49], in sharp contrast to the evolution predicted by our calculations for the same parameters and initial conditions. It is worth noting, nonetheless, that disagreements of this nature are somewhat expected to occur: for the identical frequencies case there exists a one-parameter family of invariant manifolds (of which the OA manifold is a special solution) that are neutrally stable with respect to perturbations in directions transverse to themselves [40,46,52,53]. Hence, there could be certain types of perturbations that may drive the system away from the manifold contemplated by the OA ansatz, thus generating unexpected results such as the ones discussed in Sec. VI. Another deviation from the theory was observed in the appearance of zero-lag sync and π-states over a region in the parameter space initially believed to manifest traveling waves solely [see Fig. 4(c)]. Future works should further investigate the emergence of chimeras and other states with respect to perturbations off the OA manifold for populations of identical oscillators coupled asymmetrically; the framework introduced in Ref. [50] offers a promising way to approach this problem.

As mentioned in the introduction, there are many systems whose dynamics can be modeled by phase oscillators interacting via positive and negative couplings. Our results can thereby serve as a guide in the search for clustered states in different contexts. For instance, as shown in Ref. [38], phase attraction or phase repulsion alone cannot account for the regulation of circadian rhythms; a phase model incorporating mixed couplings linked asymmetrically, on the other hand, does reproduce the outcome of experiments with neuronal networks of the SCN. Therefore, system (1) with two intertwined subpopulations may be a suitable model to describe the synchronization between the dorsal and ventral subregions of the SCN [38].

The multistable behavior of our model certainly calls for an analysis of the basins of attraction of the several states we observed. This problem can be tackled by following the methodologies in Refs. [54,55]; these possibilities, however, we leave for future works. Finally, there are a number of potentially relevant extensions for the present model: given the nontrivial behavior uncovered here, it would be interesting, for instance, to investigate more than two coupled populations, as well as to study the effect of attractive and repulsive interactions on the collective dynamics of oscillators with higher-order harmonics in the coupling function [56,57]. In particular, preliminary results (not shown here) with multipopulation systems reveal that the number of distinct TW states may grow exponentially with the number of subpopulations. For instance, for a three-subpopulation system, there may be TWs in which one subpopulation rotates, while the other two remain fully synced and static, and vice versa. One could also consider oscillators coupled on structures that allow interactions beyond the classical pairwise, such as hypergraphs [58] and simplicial complexes [59]. On the experimental domain, realizations of the dynamical transitions reported here may be obtained in populations of chemical [60,61] and optical arrays [62], which are experimental

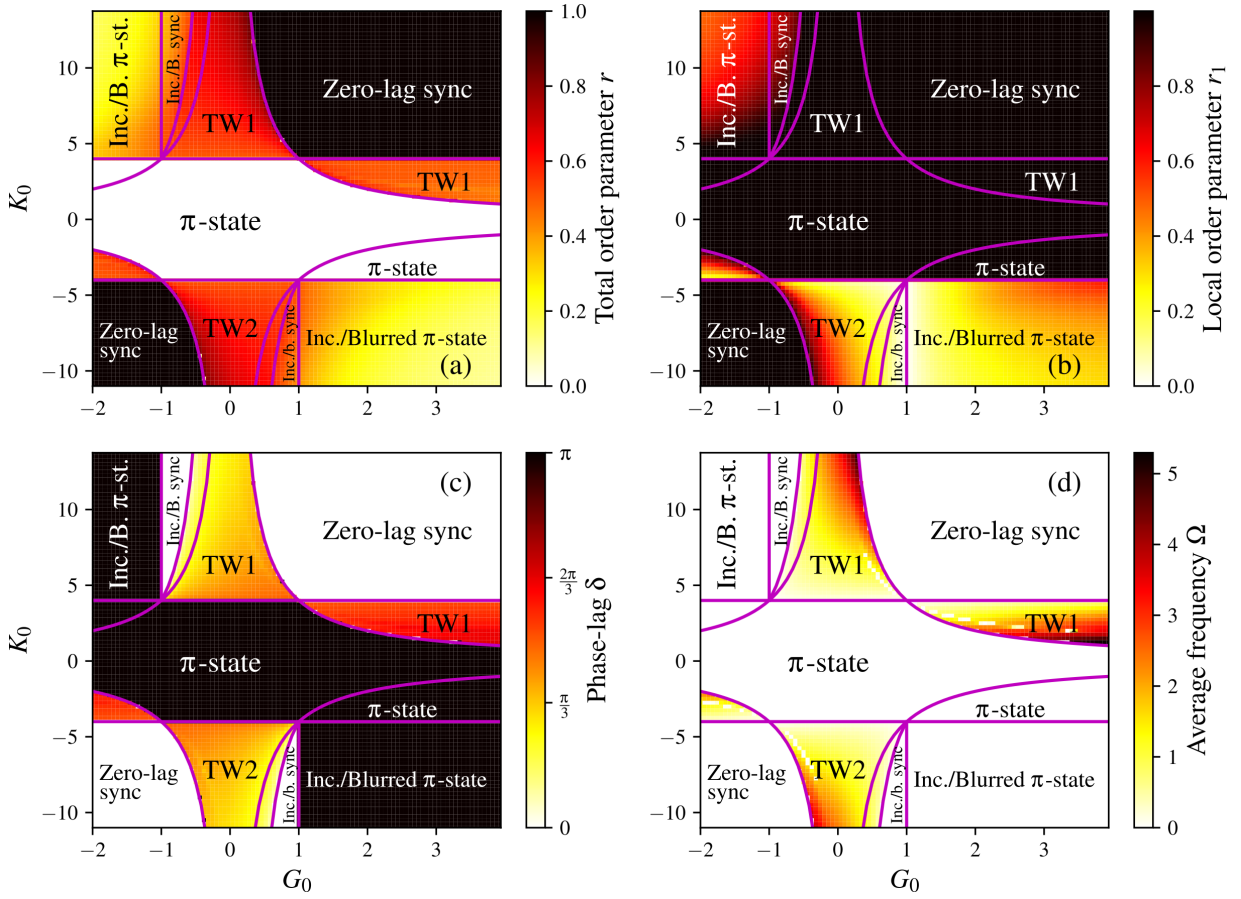

FIG. 8. Comparison between simulations (colormaps) and theory (solid lines). (a) Total order parameter r; (b) local order parameter r_1 of subpopulation 1; (c) phase lag δ measuring the separation between the two subpopulations; and (d) average frequency Ω [Eq. (14)]. For each pair of couplings (G_0, K_0), Eq. (1) are integrated numerically with the Heun's method considering $N = 10^4$ oscillators and with an integration time step $dt = 0.005$. The long-time behavior of each parameter is quantified by averaging the trajectories over $t \in [500, 1000]$. For all coupling pairs (G_0, K_0), Eq. (1) is initiated with the exact same configuration for $\theta_i(t = 0)$: phases in subpopulation 1 were randomly chosen from a Gaussian distribution with mean $\theta_1 \simeq 0.17$ and standard deviation $\sigma_1 \simeq 0.85$, yielding $r_1(t = 0) \simeq 0.69$; phases of subpopulation 2 were also Gaussian distributed, but with mean $\theta_2 \simeq 1.09$ and standard deviation $\sigma_2 \simeq 1.053$, yielding $r_2(t = 0) \simeq 0.57$. Coupling mismatch parameters: $\Delta K = 8$ and $\Delta G = 2$. $G_0 \times K_0$ grid resolution: 100×100 couplings.

setups that have been shown to reproduce chimeras and other dynamical states found in phase oscillator models.

ACKNOWLEDGMENTS

The author thanks B. Sonnenschein, C. C. Gong, D. Eroglu, P. Schultz, V. Sciuti, and B. Messias for useful conversations. This research was funded by FAPESP (Grant No. 2016/23827-6) and carried out using the computational resources of the Center for Mathematical Sciences Applied to Industry (CeMEAI) funded by FAPESP (Grant No. 2013/07375-0).

APPENDIX: SUPPLEMENTAL DIAGRAM

In this Appendix we recalculate the diagrams of Fig. 5 by initiating the oscillators differently than in Sec. V. Specifically, in Fig. 8 we choose the phases of each subpopulation to be distributed according to distinct Gaussian distributions whose peaks are separated by a phase lag (see the caption of Fig. 8 for details). Comparing Fig. 5 with Fig. 8 we see that a blurred π-state region in the former is converted into a π-state area in the latter [notice the regions with $r_1 = 0$ in Fig. 5(b) and $r_1 = 1$ in Fig. 8(b)]. In addition to the bistability between TWs and blurred zero-lag sync states confirmed in Sec. VI, another significant difference between Fig. 5 and Fig. 8 lies in the "Incoherence/Blurred π-state" areas: in Fig. 5 these regions exhibit small values for the order parameters (a consequence of choosing the initial conditions uniformly at random between $[-\pi, \pi]$), along with $\delta = \pi$; in Fig. 8, on the other hand, we observe higher values for r_1, thus confirming that multiple local synchronization levels are possible in those regions as revealed by the analysis in Sec. IV.

[1] J. A. Acebrón, L. L. Bonilla, C. J. P. Vicente, F. Ritort, and R. Spigler, The Kuramoto model: A simple paradigm for synchronization phenomena, Rev. Mod. Phys. **77**, 137 (2005).

[2] F. A Rodrigues, T. K. DM. Peron, P. Ji, and J. Kurths, The Kuramoto model in complex networks, Phys. Rep. **610**, 1 (2016).

[3] A. Arenas, A. Díaz-Guilera, J. Kurths, Y. Moreno, and C. Zhou, Synchronization in complex networks, Phys. Rep. **469**, 93 (2008).

[4] A. T. Winfree, Biological rhythms and the behavior of populations of coupled oscillators, J. Theor. Biol. **16**, 15 (1967).

[5] G. Heinrich, M. Ludwig, J. Qian, B. Kubala, and F. Marquardt, Collective Dynamics in Optomechanical Arrays, Phys. Rev. Lett. **107**, 043603 (2011).

[6] K. Wiesenfeld, P. Colet, and S. H. Strogatz, Synchronization Transitions in A Disordered Josephson Series Array, Phys. Rev. Lett. **76**, 404 (1996).

[7] I. Z. Kiss, Y. Zhai, and J. L. Hudson, Emerging coherence in a population of chemical oscillators, Science **296**, 1676 (2002).

[8] F. Dörfler and F. Bullo, Synchronization in complex networks of phase oscillators: A survey, Automatica **50**, 1539 (2014).

[9] S. Shahal, A. Wurzberg, I. Sibony, H. Duadi, E. Shniderman, D. Weymouth, N. Davidson, and M. Fridman, Synchronization of complex human networks, Nat. Commun. **11**, 1 (2020).

[10] H. Daido, Quasientrainment and Slow Relaxation in a Population of Oscillators With Random and Frustrated Interactions, Phys. Rev. Lett. **68**, 1073 (1992).

[11] L. L. Bonilla, C. J. P. Vicente, and J. M. Rubi, Glassy synchronization in a population of coupled oscillators, J. Stat. Phys. **70**, 921 (1993).

[12] J. C. Stiller and G. Radons, Dynamics of nonlinear oscillators with random interactions, Phys. Rev. E **58**, 1789 (1998).

[13] H. Daido, Algebraic relaxation of an order parameter in randomly coupled limit-cycle oscillators, Phys. Rev. E **61**, 2145 (2000).

[14] J. C. Stiller and G. Radons, Self-averaging of an order parameter in randomly coupled limit-cycle oscillators, Phys. Rev. E **61**, 2148 (2000).

[15] D. Iatsenko, P. V. E. McClintock, and A. Stefanovska, Glassy states and super-relaxation in populations of coupled phase oscillators, Nat. Commun. **5**, 4118 (2014).

[16] D. H. Zanette, Synchronization and frustration in oscillator networks with attractive and repulsive interactions, Europhys. Lett. **72**, 190 (2005).

[17] H. Hong and S. H. Strogatz, Kuramoto Model of Coupled Oscillators With Positive and Negative Coupling Parameters: An Example of Conformist and Contrarian Oscillators, Phys. Rev. Lett. **106**, 054102 (2011).

[18] H. Hong and S. H. Strogatz, Conformists and contrarians in a Kuramoto model with identical natural frequencies, Phys. Rev. E **84**, 046202 (2011).

[19] H. Hong and S. H. Strogatz, Mean-field behavior in coupled oscillators with attractive and repulsive interactions, Phys. Rev. E **85**, 056210 (2012).

[20] E. Montbrió and D. Pazó, Collective synchronization in the presence of reactive coupling and shear diversity, Phys. Rev. E **84**, 046206 (2011).

[21] D. Iatsenko, S. Petkoski, P. V. E. McClintock, and A. Stefanovska, Stationary and Traveling Wave States of the Kuramoto Model With an Arbitrary Distribution of Frequencies and Coupling Strengths, Phys. Rev. Lett. **110**, 064101 (2013).

[22] H. Hong, Periodic synchronization and chimera in conformist and contrarian oscillators, Phys. Rev. E **89**, 062924 (2014).

[23] I. M. Kloumann, I. M. Lizarraga, and S. H. Strogatz, Phase diagram for the Kuramoto model with van Hemmen interactions, Phys. Rev. E **89**, 012904 (2014).

[24] B. Sonnenschein, T. K. DM. Peron, F. A. Rodrigues, J. Kurths, and L. Schimansky-Geier, Collective dynamics in two populations of noisy oscillators with asymmetric interactions, Phys. Rev. E **91**, 062910 (2015).

[25] E. A. Martens, C. Bick, and M. J. Panaggio, Chimera states in two populations with heterogeneous phase-lag, Chaos **26**, 094819 (2016).

[26] K. P. O'Keeffe, H. Hong, and S. H. Strogatz, Oscillators that sync and swarm, Nat. Commun. **8**, 1 (2017).

[27] B. Ottino-Löffler and S. H. Strogatz, Volcano Transition in a Solvable Model of Frustrated Oscillators, Phys. Rev. Lett. **120**, 264102 (2018).

[28] J. Park and B. Kahng, Metastable state en route to traveling-wave synchronization state, Phys. Rev. E **97**, 020203 (2018).

[29] D. Anderson, A. Tenzer, G. Barlev, M. Girvan, T. M. Antonsen, and E. Ott, Multiscale dynamics in communities of phase oscillators, Chaos **22**, 013102 (2012).

[30] N. Frolov, V. Maksimenko, S. Majhi, S. Rakshit, D. Ghosh, and A. Hramov, Chimera-like behavior in a heterogeneous Kuramoto model: The interplay between attractive and repulsive coupling, Chaos **30**, 081102 (2020).

[31] J. Park and B. Kahng, Competing synchronization on random networks, J. Stat. Mech.: Theory Exp. (2020) 073407.

[32] S. Majhi, S. N. Chowdhury, and D. Ghosh, Perspective on attractive-repulsive interactions in dynamical networks: Progress and future, Europhys. Lett. **132**, 20001 (2020).

[33] B. Sonnenschein and L. Schimansky-Geier, Approximate solution to the stochastic Kuramoto model, Phys. Rev. E **88**, 052111 (2013).

[34] C. Tradonsky, M. Nixon, E. Ronen, V. Pal, R. Chriki, A. A. Friesem, and N. Davidson, Conversion of out-of-phase to in-phase order in coupled laser arrays with second harmonics, Photonics Res. **3**, 77 (2015).

[35] V. Pal, S. Mahler, C. Tradonsky, A. A. Friesem, and N. Davidson, Rapid fair sampling of the *XY* spin Hamiltonian with a laser simulator, Phys. Rev. Research **2**, 033008 (2020).

[36] H. Kori, I. Z. Kiss, S. Jain, and J. L. Hudson, Partial synchronization of relaxation oscillators with repulsive coupling in autocatalytic integrate-and-fire model and electrochemical experiments, Chaos **28**, 045111 (2018).

[37] M. Sebek and I. Z. Kiss, Plasticity facilitates pattern selection of networks of chemical oscillations, Chaos **29**, 083117 (2019).

[38] J. Myung, S. Hong, D. DeWoskin, E. De Schutter, D. B. Forger, and T. Takumi, Gaba-mediated repulsive coupling between circadian clock neurons in the SCN encodes seasonal time, Proc. Natl. Acad. Sci. USA **112**, E3920 (2015).

[39] E. Ott and T. M. Antonsen, Low dimensional behavior of large systems of globally coupled oscillators, Chaos **18**, 037113 (2008).

[40] A. Pikovsky and M. Rosenblum, Dynamics of globally coupled oscillators: Progress and perspectives, Chaos **25**, 097616 (2015).

[41] J. M. Meylahn, Two-community noisy Kuramoto model, Nonlinearity **33**, 1847 (2020).

[42] V. Vlasov, E. E. N. Macau, and A. Pikovsky, Synchronization of oscillators in a Kuramoto-type model with generic coupling, Chaos **24**, 023120 (2014).

[43] H. Sakaguchi and Y. Kuramoto, A soluble active rotater model showing phase transitions via mutual entertainment, Prog. Theor. Phys. **76**, 576 (1986).

[44] T. K. DM. Peron, J. Kurths, F. A. Rodrigues, L. Schimansky-Geier, and B. Sonnenschein, Traveling phase waves in asymmetric networks of noisy chaotic attractors, Phys. Rev. E **94**, 042210 (2016).

[45] S. Watanabe and S. H. Strogatz, Constants of motion for superconducting Josephson arrays, Physica D **74**, 197 (1994).

[46] A. Pikovsky and M. Rosenblum, Partially Integrable Dynamics of Hierarchical Populations of Coupled Oscillators, Phys. Rev. Lett. **101**, 264103 (2008).

[47] C. Bick, M. Goodfellow, C. R. Laing, and E. A. Martens, Understanding the dynamics of biological and neural oscillator networks through exact mean-field reductions: A review, J. Math. Neurosci. **10**, 1 (2020).

[48] S. Petkoski, D. Iatsenko, L. Basnarkov, and A. Stefanovska, Mean-field and mean-ensemble frequencies of a system of coupled oscillators, Phys. Rev. E **87**, 032908 (2013).

[49] D. M. Abrams, R. Mirollo, S. H. Strogatz, and D. A. Wiley, Solvable Model for Chimera States of Coupled Oscillators, Phys. Rev. Lett. **101**, 084103 (2008).

[50] J. R. Engelbrecht and R. Mirollo, Is the Ott-Antonsen manifold attracting? Phys. Rev. Research **2**, 023057 (2020).

[51] B. Pietras, N. Deschle, and A. Daffertshofer, Equivalence of coupled networks and networks with multimodal frequency distributions: Conditions for the bimodal and trimodal case, Phys. Rev. E **94**, 052211 (2016).

[52] E. A. Martens, Bistable chimera attractors on a triangular network of oscillator populations, Phys. Rev. E **82**, 016216 (2010).

[53] S. A. Marvel, R. E. Mirollo, and S. H. Strogatz, Identical phase oscillators with global sinusoidal coupling evolve by Möbius group action, Chaos **19**, 043104 (2009).

[54] E. A. Martens, M. J. Panaggio, and D. M. Abrams, Basins of attraction for chimera states, New J. Phys. **18**, 022002 (2016).

[55] P. Schultz, P. J. Menck, J. Heitzig, and J. Kurths, Potentials and limits to basin stability estimation, New J. Phys. **19**, 023005 (2017).

[56] C. C. Gong and A. Pikovsky, Low-dimensional dynamics for higher-order harmonic, globally coupled phase-oscillator ensembles, Phys. Rev. E **100**, 062210 (2019).

[57] P. S. Skardal and A. Arenas, Abrupt Desynchronization and Extensive Multistability in Globally Coupled Oscillator Simplexes, Phys. Rev. Lett. **122**, 248301 (2019).

[58] G. F. de Arruda, G. Petri, and Y. Moreno, Social contagion models on hypergraphs, Phys. Rev. Research **2**, 023032 (2020).

[59] A. P. Millán, J. J. Torres, and G. Bianconi, Explosive Higher-Order Kuramoto Dynamics on Simplicial Complexes, Phys. Rev. Lett. **124**, 218301 (2020).

[60] J. F. Totz, J. Rode, M. R. Tinsley, K. Showalter, and H. Engel, Spiral wave chimera states in large populations of coupled chemical oscillators, Nat. Phys. **14**, 282 (2018).

[61] D. Călugăru, J. F. Totz, E. A. Martens, and H. Engel, First-order synchronization transition in a large population of strongly coupled relaxation oscillators, Sci. Adv. **6**, eabb2637 (2020).

[62] A. M. Hagerstrom, T. E. Murphy, R. Roy, P. Hövel, I. Omelchenko, and E. Schöll, Experimental observation of chimeras in coupled-map lattices, Nat. Phys. **8**, 658 (2012).